Journal of Materials Chemistry C

PAPER

View Article Online
View Journal | View Issue

Cite this: J. Mater. Chem. C, 2018, 6, 5651

Gate-tunable interfacial properties of in-plane ML MX_2 1T′–2H heterojunctions†

Shiqi Liu, ‡[a] Jingzhen Li,‡[a] Bowen Shi,[a] Xiuying Zhang, [a] Yuanyuan Pan,[a] Meng Ye,[a] Ruge Quhe, [b] Yangyang Wang, [ac] Han Zhang,[a] Jiahuan Yan, [a] Linqiang Xu,[a] Ying Guo,[d] Feng Pan *[e] and Jing Lu*[af]

Received 6th March 2018,
Accepted 19th April 2018

DOI: 10.1039/c8tc01106k

rsc.li/materials-c

The two-dimensional (2D) transition-metal dichalcogenides (TMDs) field effect transistor (FET) with in-plane heterojunction contacts between the semiconducting 2H phase (as channel) and the metallic 1T or semi-metallic 1T′ phase (as electrode) has received much recent attention because it has significantly reduced contact resistance and enhanced gate tunability and thus improved device performance. However, the underlying mechanism of its good conductivity remains open. We systematically explore for the first time the contact properties of the monolayer (ML) 2H MX_2 (MoS_2, WS_2, $MoSe_2$, WSe_2, $MoTe_2$) FET with their 1T′ phase as electrode by using *ab initio* quantum transport simulations. We find that the metal induced gap states (MIGS) at the interface penetrate the Schottky barrier and bridge the electrodes and the conduction/valence band of the channel, thereby forming a lower and tunable effective Schottky barrier height (ESBH) and causing an equivalent Ohmic contact under the appropriate gate voltage. Our study provides a new insight into the observed reduced contact resistance with the 1T′ phase as electrode and is instructive for further experiment.

Introduction

Traditional three-dimensional (3D) field effect transistors (FET) are approaching their physical limit.[1–3] The shortened channel brings about the performance degradation. To overcome this problem, the channel must be thin enough to realize good control of the gate. On account of atomic thickness and a few dangling bonds at the interface, two dimensional (2D) semiconducting materials exhibit excellent gate controllability and an efficient transportation of carriers and are considered as competitive channel material for next-generation electronics.[4–7] So far, the 2H phase of transition-metal dichalcogenides (TMDs) has been the most extensively studied 2D semiconducting material.

In a practical 2D semiconductor device, the bulk metal electrode is often used to contact directly the 2D semiconducting materials to inject carriers due to lack of a substitutional doping method for 2D material.[8] Unfortunately, the Schottky barrier is usually formed at the interface of the conventional 3D metal (as electrode)-2D TMDs (as channel) semiconductor junction because of the Fermi level pinning (FLP) induced by metal induced gate states (MIGS).[9–11] The Schottky barrier at the interface causes a large contact resistance and thus a poor device performance.[11–14] Finding a new electrode with a small contact resistance (or a small Schottky barrier height (SBH)) is critical for the device application of TMDs. There are meta-stable metallic 1T and semi-metallic 1T′ allotropic phases for the stable semiconducting 2H phase of TMDs, as shown in Fig. 1.[15–17] Such an 1T′/1T phase and the 2H phase can form a seamless heterojunction, which has been experimentally fabricated by phase transition with mechanical strain,[17,18] the chemical method,[19–22] laser inducing[23] or electrostatic gating.[24] Remarkably, the 1T′/1T–2H MoS_2 and 1T′–2H $MoTe_2$ phase contact transistors exhibit a lower contact resistance, a higher carrier mobility, and an improved device performance compared with the bulk metal electrode.[15,23,25] The observed lower and gate-tunable SBH[25–27] in the 1T′/1T–2H

[a] State Key Laboratory for Mesoscopic Physics and Department of Physics, Peking University, Beijing 100871, P. R. China. E-mail: jinglu@pku.edu.cn
[b] State Key Laboratory of Information Photonics and Optical Communications and School of Science, Beijing University of Posts and Telecommunications, Beijing 100876, P. R. China
[c] Nanophotonics and Optoelectronics Research Center, Qian Xuesen Laboratory of Space Technology, China Academy of Space Technology, Beijing 100094, P. R. China
[d] School of Physics and Telecommunication Engineering, Shaanxi Sci-Tech University, Hanzhong 723001, P. R. China
[e] School of Advanced Materials, Peking University, Shenzhen Graduate School, Shenzhen 518055, P. R. China. E-mail: panfeng@pkusz.edu.cn
[f] Collaborative Innovation Center of Quantum Matter, Beijing 100871, P. R. China

† Electronic supplementary information (ESI) available: Interfacial structures of the contact configuration for the ML MoS_2 1T–2H in-plane and the ML MX_2 1T′–2H in-plane heterojunctions; energy- and space-dependent typical charge density of the MIGS in the ML $MoTe_2$ and WS_2 1T′–2H in-plane heterojunctions; comparison between of the SBHs obtained for the work function approximation for the ML MoS_2 1T–2H in-plane and the ML MX_2 1T′–2H in-plane heterojunctions in this work and Wei's work; comparison of the band structure and the transport SBH of the ML $MoTe_2$ 1T′–2H in-plane heterojunction without and with SOC. See DOI: 10.1039/c8tc01106k

‡ These authors contributed equally to this work.

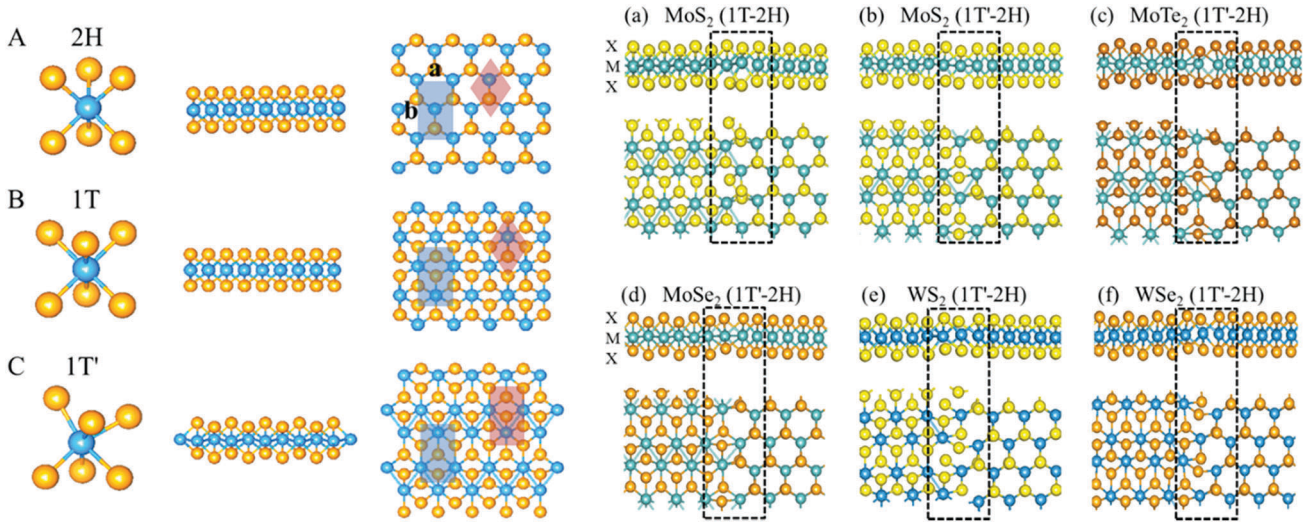

Fig. 1 Lattice structures of monolayer (A) 2H, (B) 1T and (C) 1T′ MX_2 and optimized heterojunctions ((a–f)). The blue atoms are transition metal atoms (M) and the orange atoms are chalcogenide atoms (X). The semiconducting 2H phase has a trigonal prismatic structure, and the metallic 1T and semi-metallic 1T′ phases have octahedral and distorted octahedral structures, respectively. The middle and right pictures of (A)/(B)/(C) represent the side and top views of the structures, respectively. The grey shadow represents a rectangular computational cell with the dimensions $a \times b$, and the red shadow represents the primitive cell. (a–f) Interfacial structure of the optimized contact configuration for the ML MoS_2 1T–2H and MX_2 1T′–2H in-plane heterojunctions. The apparent deformation area at the interface is zoomed in the rectangular black dash line.

MoS_2 and 1T′–2H $MoTe_2$ phase contact is believed to account for the lower contact resistance, while the underlying mechanism of the gate-tunable lower SBH remains unknown.

In this study, we explore systematically for the first time the contact properties of the in-plane Schottky-barrier field-effect transistors based on 1T′–2H heterojunctions of monolayer (ML) MX_2 (MoS_2, $MoTe_2$, $MoSe_2$, WS_2, and WSe_2) by using the density functional theory (DFT) coupled with the non-equilibrium Green's function method (NEGF). The 1T′ electrode is more common than the 1T electrode experimentally, since the 1T′ phase is more stable than the 1T phase theoretically.[21,28] In light of the experimental existence,[25,27] the 1T phase of ML MoS_2 is also investigated. We find that the Schottky barrier is always formed at the 1T′/1T–2H interface under zero gate and zero bias voltage for all the devices. However, the effective SBH is reduced because the MIGS penetrate the Schottky barrier and bridge the conduction/valence band of the channel and the electrodes, and the smallest effective hole SBH (0.20 eV) appears in the ML in-plane 1T′–2H $MoTe_2$ device. Dramatically, the effective SBH is tunable by a gate voltage, and an Ohmic contact can be achieved with the appropriate gate voltage. Such a gate tunable effective SBH is in agreement with experiment.[25,26] Our study highlights the positive role of MIGS and provides an explanation for the good performance of the Schottky-barrier field-effect transistors based on the 1T′/1T–2H heterojunctions of ML MX_2.

Computational details

We model the ML MX_2 in-plane 1T′–2H heterojunction by using the six periodic 1T′ MX_2 phase to connect its six periodic 2H phase in the lateral direction. Here we use 1T′ phase to match 2H phase to ensure the heterojunction's joint with the intrinsic 2H channel. The lattice constants of 1T′–2H heterojunctions and their mismatches at a range of 0.4–5.1% along the z direction are listed in Table 1. A vacuum buffer space of at least 15 Å is set at the x and z directions to ensure decoupling between neighboring slabs. The interaction distance between the different phases is mainly within three period lengths, so the cell shape and the outmost three periodic atoms are fixed.

The geometry optimization of the in-plane 1T′–2H heterojunction is performed using the projector-augmented wave (PAW)[29,30] pseudopotential and a plane-wave cut-off energy of 500 eV implemented in the Vienna ab initio simulation package (VASP) code.[30–34] A Γ-centered grid of $5 \times 3 \times 1$ k-points is used to sample the Brillouin zone[34] in the structural optimization. The maximum force is less than 10^{-2} eV Å^{-1} per atom, and the energy is converged to within 10^{-5} eV between two successive steps. Dipole correction is used in the z direction.

The double gated two-probe model of a ML MX_2 1T/1T′–2H phase contact transistor (Fig. 4) is built with the semiconducting 2H phase as the channel and the metallic 1T or semi-metallic 1T′ phase as the electrodes. The channel length is about 5 nm, which is enough to reproduce the observed SBHs of the 2D semiconductor FETs in terms of our previous studies.[9,35,36] The lengths of the left and right electrodes are semi-infinite. The transport properties are calculated by using DFT coupled with the non-equilibrium Green′s function (NEGF) method, which are implemented in the Atomistix ToolKit (ATK) 2016 package.[37–39] The transmission coefficient $T^{k_{//}}(E)$ ($k_{//}$ is a reciprocal lattice vector point along a surface-parallel direction (orthogonal to the transmission direction) in the irreducible Brillouin zone (IBZ)) is calculated as

$$T^{k_{//}}(E) = \mathrm{Tr}\left[\Gamma_{\mathrm{L}}^{k_{//}}(E) G^{k_{//}}(E) \Gamma_{\mathrm{R}}^{k_{//}}(E) G^{k_{//}\dagger}(E)\right] \quad (1)$$

Table 1 Calculated interfacial properties of the ML MX_2 in-plane 1T′/1T–2H heterojunction. The lattice constants b is presented according to the order $b_{1T'/1T}/b_{2H}$ ($b_{heterojunction}$). The mismatch $\bar{\varepsilon}$ of the 1T′/1T–2H phases of different 2D MX_2 materials is along the z (see Fig. 4) direction. The SBH of the electron and hole are compared respectively between the work function approximation and the quantum transport simulation in this table. E_g is the bandgap of the 2H phase. Φ_W^e and Φ_W^h are the electron and hole SBH given by the work function approximation, respectively. $\Phi_T^{e,intri}$ and $\Phi_T^{h,intri}$ are the intrinsic electron and hole SBH given by the quantum transport simulation, respectively. $\Phi_T^{e,eff}$ and $\Phi_T^{h,eff}$ are the effective electron and hole SBH given by the quantum transport simulation, respectively

	(1T–2H)	(1T′–2H)				
Contact	MoS_2	MoS_2	$MoTe_2$	$MoSe_2$	WS_2	WSe_2
b (Å)	5.49/5.47 (5.47)	5.73/5.47 (5.47)	6.33/6.10 (6.10)	5.97/5.69 (5.69)	5.73/5.46 (5.46)	5.97/5.68 (5.68)
$\bar{\varepsilon}$ (%)	0.4	4.8	3.8	4.9	4.9	5.1
E_g (2H)	1.70	1.70	1.10	1.52	1.90	1.62
Φ_W^e (eV)	0.42	1.17	0.76	1.02	1.35	1.09
Φ_W^h (eV)	1.27	0.52	0.34	0.50	0.55	0.53
$\Phi_T^{e,intri}$ (eV)	0.83	0.75	0.50	0.65	1.10	1.00
$\Phi_T^{h,intri}$ (eV)	0.90	0.6	0.50	0.60	0.90	0.82
$\Phi_T^{e,eff}$ (eV)	0.83	0.75	0.50	0.65	1.10	1.00
$\Phi_T^{h,eff}$ (eV)	0.90	0.40	0.20	0.45	0.30	0.44

where, $G^{k_{//}}$ is the retarded (advanced) Green's function and $\Gamma_{L/R}^{k_{//}}(E) = i\left(\Sigma_{L/R}^{r,k_{//}} - \Sigma_{L/R}^{a,k_{//}}\right)$ represents the level broadening due to the left electrodes and the right electrodes expressed in terms of the electrode self-energies $\Sigma_{L/R}^{k_{//}}$, which reflects the influence of the electrodes on the scattering region. The transmission function at a given energy $T(E)$ is averaged over different $k_{//}$ in the IBZ. The double-ζ-polarized (DZP) basis set is employed. The real-space mesh cutoff is of 75 Hartree, and the temperature is set at 300 K. The electronic structures of the electrodes and central region are calculated with a Monkhorst–Pack 1 × 32 × 32 and 1 × 32 × 20 k-point grids, respectively. A periodic type, a Neumann type and a Dirichlet type boundary condition are used in the x, y and z directions of the device (Fig. 4), respectively. Generalized gradient approximation (GGA) of the Perdew–Burke–Ernzerhof (PBE)[40] form to the exchange–correlation functional is applied throughout this paper.

Because the electron–electron interaction of the 2D semiconductor channel is greatly screened by doped carriers from the metal electrode, single-electron-approximation based on DFT-GGA is effective enough to evaluate the SBH in a FET configuration.[41,42] Indeed, for a degenerately doped ML $MoSe_2$, the band gap of 1.52 eV at DFT-GGA level is in good agreement with the renormalized band gap of 1.59 eV obtained by the GW method[42] and the experimental result of 1.58 eV.[43] For another example, the experimental transport gap of the ML, bilayer (BL), and trilayer (TL) black phosphorene with the Ni electrode is 1.00, 0.71 and 0.61 eV, respectively, while the calculated transport gaps at the DFT-GGA level are 0.65, 0.81 and 0.68 eV, respectively.[10,36,44]

Results

Electronic structure of the ML 1T′/1T–2H MX_2 interface

Table 1 shows the optimized lattice constants of ML 1T′/1T and 2H MX_2, which are in good agreement with the previous theoretical reports.[28] In our model, MX_2 1T′/1T–2H join along their armchair edges, and experimentally the contact properties are not critically influenced by contact orientations.[26] The optimized 1T′/1T–2H interface structures are shown in Fig. 1. Compared with the initial structure (Fig. S1, ESI†), the 1T′/1T phase within one period at the interface always undergoes a substantial deformation (circled by black dashed line) while the 2H phase almost remains unchanged because the 2H phase is more stable than the 1T′/1T phase.[21]

The electronic structures of free-standing ML 2H MX_2 and ML 1T′/1T MX_2 are presented in Fig. 2 and 3, respectively. The free-standing ML 2H MX_2 shows a direct band gap ranging from 1.0 to 2.0 eV at the K point. These are consistent with the reported PBE values.[45] The 1T′ MX_2 is semi-metallic because the energy band around the Fermi level is like a Dirac cone and the density of states (DOS) at the Fermi level is approximately zero (Fig. 3).[46] Compared with ML 1T′ MX_2, ML 1T MoS_2 has a higher DOS at the Fermi level which is in accordance with its metallic characteristics.

Quantum transport simulation of the 1T′/1T–2H heterojunction

The schematic diagram of the device configuration is shown in Fig. 4. The central region of the device is the 2H channel

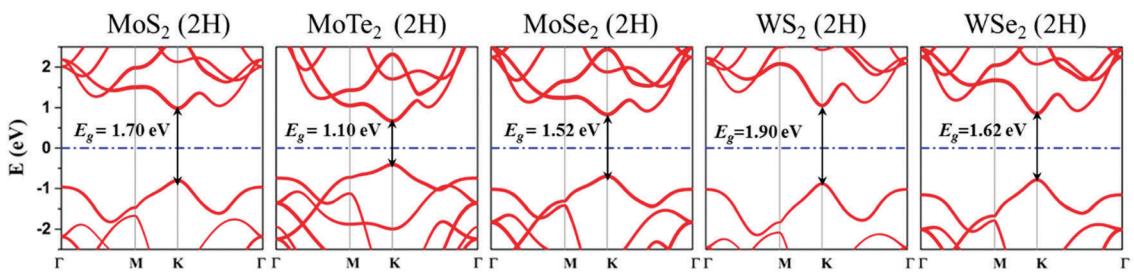

Fig. 2 Band structures of ML 2H MX_2 without the inclusion of SOC. The Fermi level is at zero energy (blue dashed line).

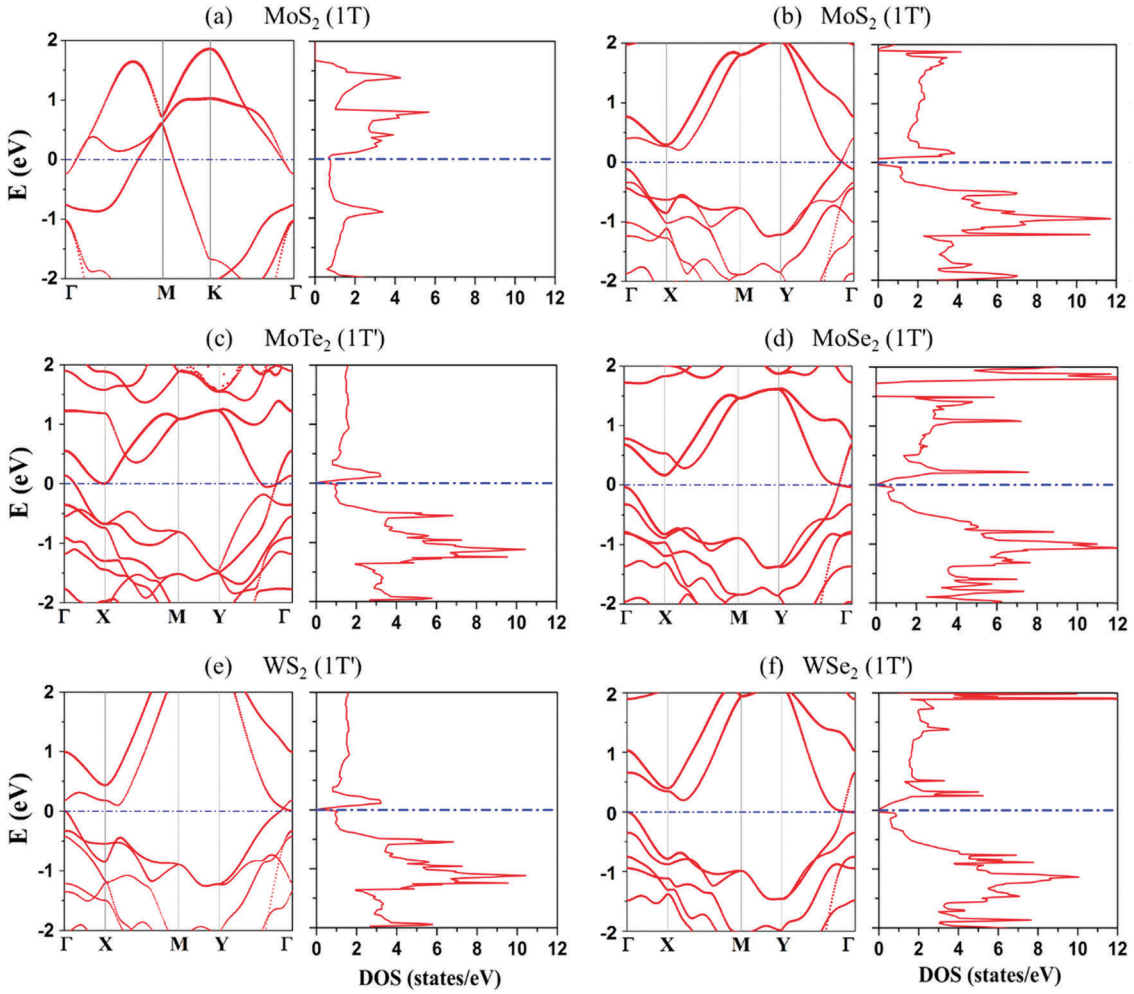

Fig. 3 (a–f) Band structures and density of states (DOS) of ML 1T MoS_2 and 1T′ MX_2 without the inclusion of SOC. The Fermi level is at zero energy (blue dashed line).

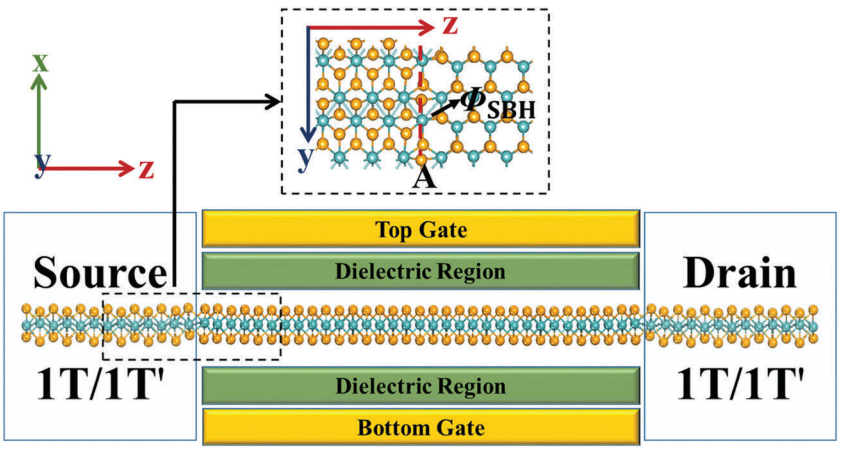

Fig. 4 Schematic diagram of a ML MX_2 in-plane transistor based on 1T′/1T–2H heterojunctions with double gates. The contact region's top view of different phases is zoomed in the top rectangular black dash line. A is the source/drain-channel interface (red dashed lines), and Φ_{SBH} represents the Schottky barrier at interface A.

(covered by gate electrode). Connected to the channel are the periodic intrinsic 1T′/1T phase MX_2, located at the devices' two sides. The 1T′/1T–2H contact interface (the transition area) has been optimized. Quantum transport simulation is a reliable

approach to determine the SBH due to the inclusion of the coupling between the electrode and the channel. Local device density of states (LDDOS) is a direct way to reflect the real space energy band distribution and MIGS in the FETs. The electron/hole SBH therefore can be extracted from the difference between the Fermi level and the CBM/VBM of the 2H phase at the interface, by virtue of the LDDOS.

SBH at zero gate voltage and zero bias

The LDDOS's and the corresponding transmission spectrum of the ML MX_2 in-plane 1T′–2H FET under V_g = 0.0 V and V_b = 0.0 V are shown in (b)–(f) of Fig. 5. We mark the intrinsic VBM (IVBM, black solid curve) according to the shape of the CBM. The Fermi level of the intrinsic 1T′ phase is always lower than that of the 2H semiconductor channel in terms of the work function calculation and electrons are transferred from the channel to the electrode at the interface. The charge redistribution leads to a built-in electric field and down-bending of the energy band in all the 2H channels. The 1T′–2H heterojunctions always turn out to be a p-type Schottky contact with the hole intrinsic SBH (ISBH) of $\Phi_T^{h,intri}$ = 0.60, 0.50, 0.60, 0.90, 0.82 eV for MoS_2, $MoTe_2$, $MoSe_2$, WS_2, WSe_2 FET, respectively.

Work function approximation (WFA) is a popular method to estimate the SBH of a FET. In the WFA, the electron/hole SBH Φ_W^e/Φ_W^h (list in Table 1) is defined as the energy difference between the Fermi level of a 1T or 1T′ electrode and the CBM/VBM of the 2H channel. This method ignores the interaction between the 2H semiconducting channel and the 1T′ metallic electrode. Our calculated SBHs from the WFA are comparable with the previous results by Wei (Fig. S3, ESI†),[45] and the same contact polarities are available. The SBHs from the WFA are compared with those from the quantum transport simulation in Table 1 and Fig. 8. The contact polarities given by the quantum transport simulation are consistent with those obtained from the WFA. However, the hole ISBHs from the quantum transport simulation are generally higher than the hole SBHs obtained by the WFA. The hole SBH reduction $\Delta\Phi^h$ is defined as $\Delta\Phi^h = \Phi_T^{h,intri} - \Phi_W^h$, and it is 0.08, 0.16, 0.10, 0.35, 0.29 eV for the ML 1T′–2H MoS_2, $MoTe_2$, $MoSe_2$, WS_2, and WSe_2 in-plane contact, respectively. The difference between the two methods reflects the Fermi level pinning (FLP) between the electrode and channel induced by the MIGS, which usually serve as a reservoir for the charge transfer between the electrode and channel. FLP not only increases the SBH but also make the SBH hard to tune by a gate voltage, thus degrading the device performance. In view of FLP, the quantum transport simulation is highly desirable in predicting the SBH in a FET.[9,36,47]

However, from the LDDOS, apparent MIGS states fill the triangle region between the energy band of 1T′ electrode and the VBM of the 2H channel at the interface (Fig. 5), which means that a new path is opened for carrier transport from the electrode to the channel. Taking the intrinsic VBM and this kind of deeply expanded MIGS as a whole, we can define an effective VBM (EVBM, white solid curve). Correspondingly, the transmission spectra also show an onset at the effective VBM position (Fig. 5). Thus an effective hole SBH ($\Phi_T^{h,eff}$) can be extracted from the EVBM. We have $\Phi_T^{h,eff}$ = 0.40, 0.20, 0.45, 0.30, 0.44 eV for the ML in-plane 1T′–2H MoS_2, $MoTe_2$, $MoSe_2$, WS_2, WSe_2 contacts, respectively, which is reduced by 0.20, 0.30, 0.15, 0.60, 0.38 eV with respect to the corresponding ISBH. The calculated small effective hole SBH of 0.20 eV in the ML $MoTe_2$ 1T′–2H contact is slightly larger than the experimental value 0.025 eV in the few-layer $MoTe_2$ 1T′–2H contact.[25] The calculated effective hole SBH will be reduced if the few-layer $MoTe_2$ 1T′–2H contact model is adopted due to the reduced band gap with the increasing layer number. On the other hand, the intrinsic hole SBH of 0.50 eV from the quantum transport simulation and the hole SBH of 0.34 eV from the work function approximation in the ML $MoTe_2$ 1T′–2H contact are much higher than the observed one.[26] This much better agreement in the SBH with the experiment from the quantum transport simulation compared with the work function approximation highlights the importance of the quantum transport simulation in predicting the SBH once more.[10,36,44,48]

As for the in-plane ML MoS_2 1T–2H FET, there are no apparent MIGS around the CBM of 2H MoS_2 at the interface (Fig. 5(a)), so the effective CBM is equal to the intrinsic CBM and thus the ESBH is equal to the ISBH. The LDDOS shows that the in-plane ML MoS_2 1T–2H contact is a n-type Schottky contact with an electron SBH of 0.83 eV. This is in good agreement with the value of 0.82 eV from a previous quantum transport calculation of the in-plane ML MoS_2 1T–2H contact.[49] The experiment shows the in-plane few layer MoS_2 1T–2H contact is an n-type Schottky contact with a small SBH of 0.13–0.18 eV at zero gate voltage.[25] There are two possible causes for this discrepancy. One is the number of layers, which plays a significant role in determining the SBH. The more the layer number, the lower the SBH. The other is doping by the contact electrode, which gives rise to the shift in the work function of the 1T phase.[50] The polarity difference between ML MoS_2 1T and 1T′–2H contact can be explained in this way: the 1T′ phase has a lower Fermi level than the 1T phase because the 1T′ phase has a lower total energy than the 1T phase. A lower Fermi level is closer to the VBM, in favor of a p-type polarity in the 1T′–2H contact, whereas a higher Fermi level is closer to the CBM, leading to an n-type polarity in the 1T–2H contact.

Tunability of the ESBH by a gate voltage

Generally, if the Schottky contact has weak or no FLP, the whole energy band of the channel can be tuned by a gate voltage and the SBH is thus tunable by a gate voltage, probably leading to an Ohmic contact.[45,51] For example, due to the weak FLP induced by depressed MIGS, the SBH of the ML black phosphorus transistor with the 2D graphene electrode is tuned from 0.3 eV to −0.05 eV as the gate voltage changes from 1.5 V to −0.5 V at V_b = 0.5 V.[51] By contrast, if the Schottky contact has a strong FLP, the Ohmic contact is usually difficult to achieve because those ending points of the energy band at the interface are fixed.[51] Namely, the SBH is almost fixed in the case of strong FLP.

We identify a strong FLP of MX_2 in-plane FET based on the 1T′–2H heterojunction because the hole ISBH obtained from the transport simulation is apparently higher than the respective hole SBH obtained from the WFA and is untunable by a

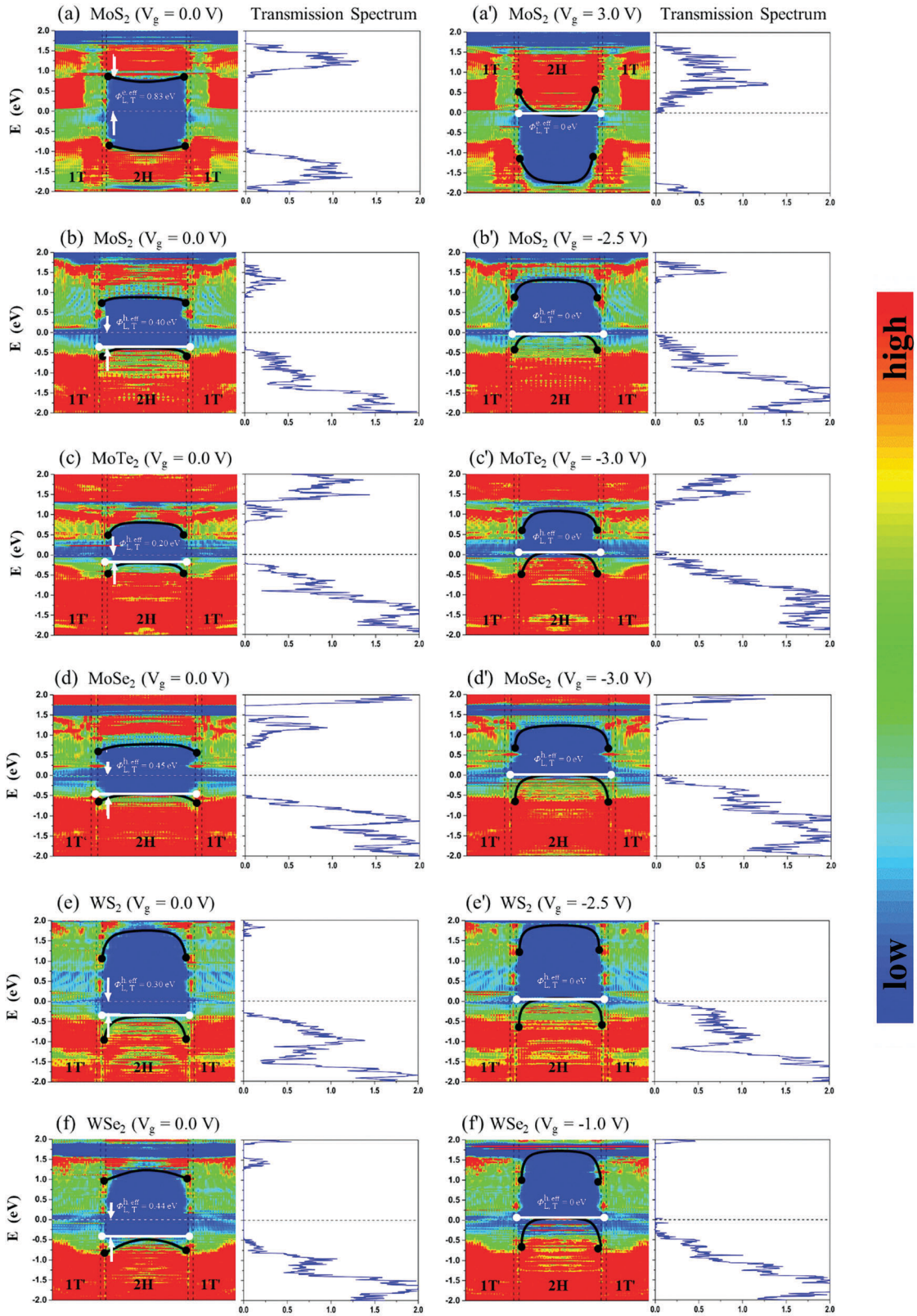

Fig. 5 LDDOS (left panel) and transmission spectra (right panel) of the ML in-plane MoS_2 1T–2H (a) and MX_2 1T′–2H ((b–f)) transistors at $V_g = 0$ (left) and $V_g \neq 0$ (right). The Fermi level is represented by a white dashed line in LDDOS and the black dashed line in the transmission spectrum. The intrinsic and effective VBM/CBM is represented by the black solid curves and white solid curve, respectively. The ISBH is marked by the black ending points of the intrinsic CBM/VBM. The ESBH is marked by the white ending points of the effective CBM/VBM, $\Phi_T^{e,eff}$ and $\Phi_T^{h,eff}$ represent the electron/hole ESBH in the source/drain-channel interface, respectively. The interface region of the 1T′ and 2H phases is shown between the upright black lines. The color scale is shown on the right side of the plot.

gate voltage. However, we find the ESBH can be tuned by a gate voltage significantly and even an Ohmic contact can be achieved with V_g = 3.0, −2.5, −3.0, −2.5, −3.0, −1.0 V for the in-plane ML 1T–2H MoS_2 and 1T′–2H MoS_2, $MoTe_2$, $MoSe_2$, WS_2, WSe_2 FET, respectively ((a′)–(f′) of Fig. 5). The MIGS that bridge the electrodes and the VBM of the channel at the interface in the in-plane ML MX_2 1T′–2H FETs are deep enough to be tuned by a gate voltage. The energy- and space-dependent typical charge density of the MIGS are shown in Fig. S2 of ESI.† Since the effective VBM consists of the intrinsic VBM at the channel region (tunable by a gate voltage) and the MIGS at the interface, it is tunable and thus the ending points of the effective VBM can be tuned to the Fermi level by the appropriate gate voltage, leading to a p-type Ohmic contact. As for the in-plane ML 1T–2H MoS_2 FET, the electron ISBH is tunable due to few MIGS at the interface, and meanwhile the gate voltage further introduces a new deeply expanded MIGS and leads to a lower electron ESBH (Fig. 5(a) and (a′)). The tunable ESBH of the MX_2 in-plane FETs based on the 1T′/1T–2H heterojunction is in good agreement with the observed effective gate tunability in the experiment,[25,26] wherein a gate change of 4 eV reduces the electron SBH from 0.13 to 0 eV in the few-layer 1T–2H MoS_2 contact. Hence, the observed good conductivity and improved device performance in the 1T′/1T–2H MoS_2[15,25] and 1T′–2H $MoTe_2$[26] phase contact transistors can be explained.

As shown in Fig. 5, in the case of the p-type Ohmic contact, the transmission spectra consistently shows an onset at the Fermi level. Fig. 6 displays the transmission eigenstates (ES) of the ML 1T′–2H $MoTe_2$ FET at E = −0.1 V and k = (0, 0) under V_g = 0.0 V and V_g = −3.0 V, respectively. At V_g = 0.0 V, we find that the incoming wave function of the eigenstate is localized at the source and is unable to go through the central channel to reach the drain (Fig. 6(a)). When the gate voltage increases to −3 eV, the effective VBM at the center 2H channel will rise and reach the Fermi level, and the wave function of the eigenstate is expanded to the channel and reaches the drain (Fig. 6(b)).

Discussion

The differences between the lattices of the 1T′ and 2H phases have been added to Table 1. In light of the sensitivity of the band gap of the 2H phase to strain, here we use the 1T′ phase to match the 2H phase to ensure the heterojunction's joint with the intrinsic 2H channel. Thus the lattice constant of the heterojunction is equal to the 2H phase. Because 1T′ phase is stretched, it probably affects the SBHs calculated by the WFA, where the SBH is the energy difference between the Fermi level of 1T or the 1T′ electrode and the CBM/VBM of the 2H channel. We chose 1T′ WSe_2, which has the maximal mismatch in our simulation and test its workfunction (Fermi level) change caused by strain. With the lattice constant stretched from 5.97 (1T′) to 5.68 Å (2H), the workfunction changes from 4.65 to 4.73 eV. This tiny difference implies that the SBH change is only as small as 0.08 eV if the 1T′ phase is not stained. Due to the Fermi level pinning at the interface, the SBH obtained by the quantum transport simulation is harder to change and thus its change is believed to be smaller than 0.08 eV if the 1T′ phase is not stained. In other words, the SBH under both the work function approximation and the quantum transport simulation is insensitive to the strain of the metallic 1T′ phase.

The schematic diagram of the Ohmic contacts is shown in Fig. 7. In our simulated system, we have demonstrated the MIGS brings about the FLP, forming the intrinsic SBH and degrading the device performance. Dramatically, with some deeply expanded MIGS penetrating the Schottky barrier and bridging the electrodes and conduction/valence band of the channel, a lower ESBH is formed so as to improve the situation. Thus the actual performance of the device depends on the competence between the two opposite effects of the MIGS. At V_g = 0.0 V and V_b = 0.0 V, though the deeply expanded MIGS do participate in forming effective VBM/CBM and lead to a lower ESBH, the FLP is masked partly but still dominates the device performance, and all the devices remain in Schottky contact. However, due to the tunability of the SBH caused by the deeply

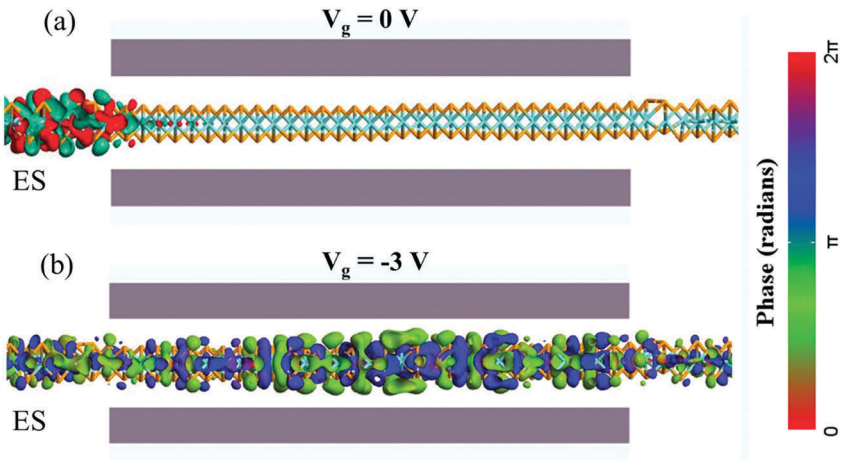

Fig. 6 Comparison of the transmission eigenstates (ES) at different gate voltages. (a): ES at the E = −0.1 V and k = (0, 0) of the Off state for the ML 1T′–2H $MoTe_2$ Schottky-barrier FET with V_g = 0 V. (b) ES at the E = −0.1 V and k = (0, 0) of the ON state for the ML 1T′–2H $MoTe_2$ Schottky-barrier FET with V_g = −3 V. The isovalues are 0.2 a.u. for the two eigenstates. The phase color scale is shown on the right of the plot.

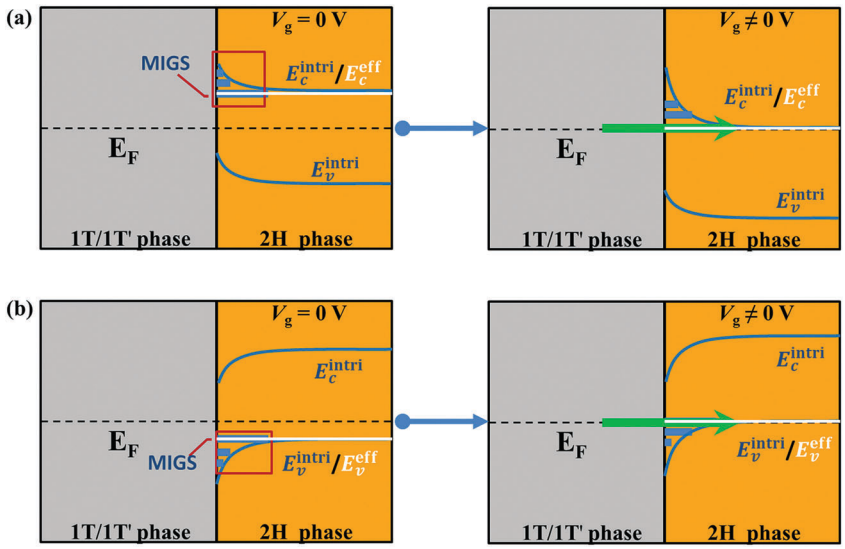

Fig. 7 Left: Illustration of the band alignment at the interfaces of the ML MX_2 1T/1T′–2H in-plane heterojunction with V_g = 0 V. E_F is the Fermi level (black dashed line). The dark blue shadow between the intrinsic CBM (E_c^{intri}) and the intrinsic VBM (E_v^{intri}) represents the MIGS. E_c^{eff}/E_v^{eff} is the effective CBM/VBM represented by white solid line, respectively. Right: Schematic diagram of Ohmic contact with the help of interface states with the appropriate gate voltage. Green arrow shows the pathway of carrier injection from the 1T/1T′ electrode to the 2H channel. (a) and (b) represent the realization procedure of the n-type and p-type Ohmic contact, respectively.

expanded MIGS, the FLP can be masked totally and an Ohmic contact can be achieved under the appropriate gate voltage.

For the MX_2 systems, the spin orbit coupling (SOC) effect could be significant, especially for the MX_2 (X = Te). So we choose $MoTe_2$ as an example to test SOC's influence on the energy gap and the transport SBH. After taking the SOC into consideration, the valence band's splitting at *K* point brings about a 0.15 eV decrease in the band gap. The quantum transport simulation only shows a 0.05 eV decrease in the effective hole-SBH (Fig. S4, ESI†). Compared with the change of the band gap, the smaller change in the effective hole SBH is attributed to the strong Fermi level pinning at the interface.

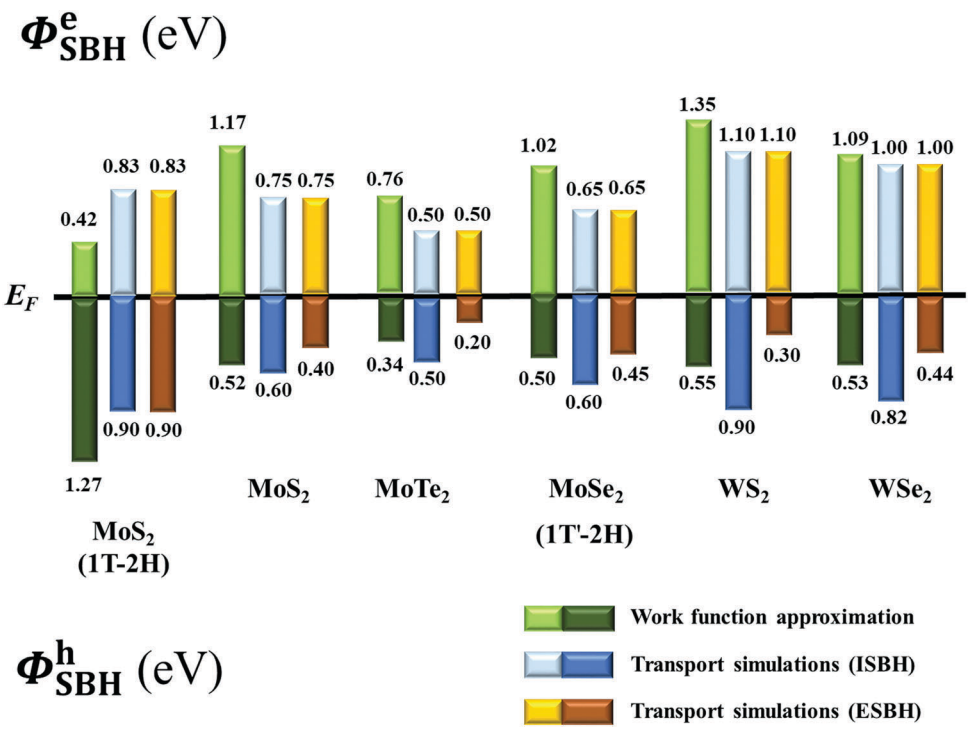

Fig. 8 Comparison of the SBH obtained from the WFA (Φ_W^e/Φ_W^h) and the quantum transport simulations ($\Phi_T^{e,intri}/\Phi_T^{h,intri}$, $\Phi_T^{e,eff}/\Phi_T^{h,eff}$) for the ML MX_2 in-plane 1T′/1T–2H phase contact transistors. The blue bar and the yellow bar represent the ISBH and the ESBH, respectively.

Thus the almost negligible change in the transport SBH implies that SOC will not affect our conclusions. The comparison of the band structure and LDDOS with and without the inclusion of SOC are shown in Fig. S4 of ESI.†

The in-plane seamless design establishes a pure contact formed by covalent bonds with atomic precision. Due to the covalent bonding happening at the interface, the coupling can be much stronger, which is consistent with the existence of the widely-dispersing and deeply expanded MIGS. The previous studies show that the device with a low-dimensional electrode always performs better than that with the bulk metal electrode due to the less screening to the gate electric fields.[51–53] Similarly, in the in-plane ML MX_2 1T′–2H EFT, the 2D 1T′ electrode is thin enough to weaken the screening effect from the electrodes and leads to improved control of the gate. Both the deeply expanded MIGS and the enhanced gate control from the 2D electrode contribute to the tunable ESBH, leading to an Ohmic contact and improved device performance in the in-plane ML MX_2 1T′–2H EFT under the appropriate gate voltage.

Conclusion

In summary, we systematically explore for the first time the contact properties of ML 2H MX_2 (MoS_2, WS_2, $MoSe_2$, WSe_2, $MoTe_2$) FET with their 1T′ phase as electrode by using *ab initio* quantum transport simulations. Because of the deeply expanded MIGS, which bridge the conduction/valence band of the channel and the electrodes, a lower effective SBH is formed. The ML $MoTe_2$ in-plane 1T′–2H contact has the lowest hole effective SBH of 0.20 eV, which is comparable with the experimental value.[26] Furthermore, an equivalent Ohmic contact can be achieved as a result of the tunable effective SBH by the appropriate gate voltage. Our study provides a new insight into the observed reduced contact resistance with the 1T′ phase as electrode.

Conflicts of interest

There are no conflicts to declare.

Acknowledgements

This work was supported by the National Natural Science Foundation of China (No. 11674005/11664026), the Ministry of Science and Technology (No. 2016YFB0700600 (National Materials Genome Project) and 2016YFA0301300) of China. We thank Prof. Li Yang and David Tomanek for helpful discussions and Prof. Manish Chhowalla for the patient reply on the experiment.

References

1 R. F. Service, Is Silicon's Reign Nearing Its End?, *Science*, 2009, **323**(5917), 1000–1002.
2 D. Xiang, X. L. Wang, C. C. Jia, T. Lee and X. F. Guo, Molecular-Scale Electronics: From Concept to Function, *Chem. Rev.*, 2016, **116**(7), 4318–4440.
3 H. Jeong, D. Kim, G. Wang, S. Park, H. Lee, K. Cho, W. T. Hwang, M. H. Yoon, Y. H. Jang, H. Song, D. Xiang and T. Lee, Redox-Induced Asymmetric Electrical Characteristics of Ferrocene- Alkanethiolate Molecular Devices on Rigid and Flexible Substrates, *Adv. Funct. Mater.*, 2014, **24**(17), 2472–2480.
4 F. Schwierz, J. Pezoldt and R. Granzner, Two-Dimensional Materials and Their Prospects in Transistor Electronics, *Nanoscale*, 2015, **7**(18), 8261–8283.
5 D. Akinwande, N. Petrone and J. Hone, Two-Dimensional Flexible Nanoelectronics, *Nat. Commun.*, 2014, **5**, 5678.
6 G. Fiori, F. Bonaccorso, G. Iannaccone, T. Palacios, D. Neumaier, A. Seabaugh, S. K. Banerjee and L. Colombo, Electronics Based on Two-Dimensional Materials, *Nat. Nanotechnol.*, 2014, **9**(12), 1063.
7 Q. H. Wang, K. Kalantar-Zadeh, A. Kis, J. N. Coleman and M. S. Strano, Electronics and Optoelectronics of Two-Dimensional Transition Metal Dichalcogenides, *Nat. Nanotechnol.*, 2012, **7**(11), 699–712.
8 S. Banerjee, J. Rowland, O. Erten and M. Randeria, Enhanced Stability of Skyrmions in Two-Dimensional Chiral Magnets with Rashba Spin–Orbit Coupling, *Phys. Rev. X*, 2014, **4**(3), 031045.
9 H. X. Zhong, R. G. Quhe, Y. Y. Wang, Z. Y. Ni, M. Ye, Z. G. Song, Y. Y. Pan, J. B. Yang, L. Yang, M. Lei, J. J. Shi and J. Lu, Interfacial Properties of Monolayer and Bilayer MoS_2 Contacts with Metals: Beyond the Energy Band Calculations, *Sci. Rep.*, 2016, **6**, 21786.
10 X. Y. Zhang, Y. Y. Pan, M. Ye, R. Quhe, Y. Y. Wang, Y. Guo, H. Zhang, Y. Dan, Z. G. Song, J. Z. Li, J. B. Yang, W. L. Guo and J. Lu, Three-layer phosphorene-metal interfaces, *Nano Res.*, 2018, **11**(2), 707–721.
11 J. H. Kang, W. Liu, D. Sarkar, D. Jena and K. Banerjee, Computational Study of Metal Contacts to Monolayer Transition-Metal Dichalcogenide Semiconductors, *Phys. Rev. X*, 2014, **4**(3), 031005.
12 C. Gong, L. Colombo, R. M. Wallace and K. Cho, The Unusual Mechanism of Partial Fermi Level Pinning at Metal-MoS_2 Interfaces, *Nano Lett.*, 2014, **14**(4), 1714–1720.
13 Y. Z. Guo, D. M. Liu and J. Robertson, 3D Behavior of Schottky Barriers of 2D Transition-Metal Dichalcogenides, *ACS Appl. Mater. Interfaces*, 2015, **7**(46), 25709–25715.
14 I. Popov, G. Seifert and D. Tomanek, Designing Electrical Contacts to MoS_2 Monolayers: A Computational Study, *Phys. Rev. Lett.*, 2012, **108**(15), 156802.
15 R. Kappera, D. Voiry, S. E. Yalcin, B. Branch, G. Gupta, A. D. Mohite and M. Chhowalla, Phase-Engineered Low-Resistance Contacts for Ultrathin MoS_2 Transistors, *Nat. Mater.*, 2014, **13**(12), 1128–1134.
16 K. F. Mak, C. Lee, J. Hone, J. Shan and T. F. Heinz, Atomically Thin MoS_2: A New Direct-Gap Semiconductor, *Phys. Rev. Lett.*, 2010, **105**(13), 136805.
17 K. A. N. Duerloo, Y. Li and E. J. Reed, Structural Phase Transitions in Two-Dimensional Mo- and W-Dichalcogenide Monolayers, *Nat. Commun.*, 2014, **5**, 4214.
18 X. Q. Lin and J. Ni, Topological Phase Transition Due to Strain-Controlled Evolution of the Inverted Bands in 1T′−MX_2, *Phys. Rev. B*, 2017, **95**(24), 245436.

19 G. Eda, T. Fujita, H. Yamaguchi, D. Voiry, M. W. Chen and M. Chhowalla, Coherent Atomic and Electronic Heterostructures of Single-Layer MoS_2, *ACS Nano*, 2012, **6**(8), 7311–7317.

20 G. P. Gao, Y. Jiao, F. X. Ma, Y. L. Jiao, E. Waclawik and A. J. Du, Charge Mediated Semiconducting-to-Metallic Phase Transition in Molybdenum Disulfide Monolayer and Hydrogen Evolution Reaction in New 1T' Phase, *J. Phys. Chem. C*, 2015, **119**(23), 13124–13128.

21 M. Kan, J. Y. Wang, X. W. Li, S. H. Zhang, Y. W. Li, Y. Kawazoe, Q. Sun and P. Jena, Structures and Phase Transition of a MoS_2 Monolayer, *J. Phys. Chem. C*, 2014, **118**(3), 1515–1522.

22 Y. M. Kang, S. Najmaei, Z. Liu, Y. J. Bao, Y. M. Wang, X. Zhu, N. J. Halas, P. Nordlander, P. M. Ajayan, J. Lou and Z. Y. Fang, Plasmonic Hot Electron Induced Structural Phase Transition in a MoS_2 Monolayer, *Adv. Mater.*, 2014, **26**(37), 6467–6471.

23 S. Cho, S. Kim, J. H. Kim, J. Zhao, J. Seok, D. H. Keum, J. Baik, D. H. Choe, K. J. Chang, K. Suenaga, S. W. Kim, Y. H. Lee and H. Yang, Phase Patterning for Ohmic Homojunction Contact in $MoTe_2$, *Science*, 2015, **349**(6248), 625–628.

24 Y. Li, K. A. N. Duerloo, K. Wauson and E. J. Reed, Structural Semiconductor-to-Semimetal Phase Transition in Two-Dimensional Materials Induced by Electrostatic Gating, *Nat. Commun.*, 2016, **7**, 10671.

25 Y. Katagiri, T. Nakamura, A. Ishii, C. Ohata, M. Hasegawa, S. Katsumoto, T. Cusati, A. Fortunelli, G. Iannaccone, G. Fiori, S. Roche and J. Haruyama, Gate-Tunable Atomically Thin Lateral MoS_2 Schottky Junction Patterned by Electron Beam, *Nano Lett.*, 2016, **16**(6), 3788–3794.

26 J. H. Sung, H. Heo, S. Si, Y. H. Kim, H. R. Noh, K. Song, J. Kim, C. S. Lee, S. Y. Seo, D. H. Kim, H. K. Kim, H. W. Yeom, T. H. Kim, S. Y. Choi, J. S. Kim and M. H. Jo, Coplanar Semiconductor-Metal Circuitry Defined on Few-Layer $MoTe_2$ *via* Polymorphic Heteroepitaxy, *Nat. Nanotechnol.*, 2017, **12**(11), 1064–1070.

27 R. Kappera, D. Voiry, S. E. Yalcin, B. Branch, G. Gupta, A. D. Mohite and M. Chhowalla, Phase-Engineered Low-Resistance Contacts for Ultrathin MoS_2 Transistors, *Nat. Mater.*, 2014, **13**(12), 1128–1134.

28 W. Zhao and F. Ding, Energetics and Kinetics of Phase Transition between a 2H and a 1T MoS_2 Monolayer-a Theoretical Study, *Nanoscale*, 2017, **9**(6), 2301–2309.

29 P. E. Blochl, Projector Augmented-Wave Method, *Phys. Rev. B: Condens. Matter Mater. Phys.*, 1994, **50**(24), 17953–17979.

30 G. Kresse and D. Joubert, From Ultrasoft Pseudopotentials to the Projector Augmented-Wave Method, *Phys. Rev. B: Condens. Matter Mater. Phys.*, 1999, **59**(3), 1758–1775.

31 G. Kresse, Ab-Initio Molecular-Dynamics for Liquid-Metals, *J. Non-Cryst. Solids*, 1995, **193**, 222–229.

32 G. Kresse and J. Furthmuller, Efficiency of Ab-Initio Total Energy Calculations for Metals and Semiconductors Using a Plane-Wave Basis Set, *Comput. Mater. Sci.*, 1996, **6**(1), 15–50.

33 G. Kresse and J. Hafner, Ab-Initio Molecular-Dynamics Simulation of the Liquid-Metal Amorphous-Semiconductor Transition in Germanium, *Phys. Rev. B: Condens. Matter Mater. Phys.*, 1994, **49**(20), 14251–14269.

34 H. J. Monkhorst and J. D. Pack, Special Points for Brillouin-Zone Integrations, *Phys. Rev. B: Solid State*, 1976, **13**(12), 5188–5192.

35 Y. Y. Pan, S. B. Li, M. Ye, R. G. Quhe, Z. G. Song, Y. Y. Wang, J. X. Zheng, F. Pan, W. L. Guo, J. B. Yang and J. Lu, Interfacial Properties of Monolayer $MoSe_2$-Metal Contacts, *J. Phys. Chem. C*, 2016, **120**(24), 13063–13070.

36 Y. Y. Pan, Y. Y. Wang, M. Ye, R. G. Quhe, H. X. Zhong, Z. G. Song, X. Y. Peng, D. P. Yu, J. B. Yang, J. J. Shi and J. Lu, Monolayer Phosphorene-Metal Contacts, *Chem. Mater.*, 2016, **28**(7), 2100–2109.

37 M. Brandbyge, J. L. Mozos, P. Ordejon, J. Taylor and K. Stokbro, Density-Functional Method for Nonequilibrium Electron Transport, *Phys. Rev. B: Condens. Matter Mater. Phys.*, 2002, **65**(16), 165401.

38 D. R. Smith, S. Schultz, P. Markos and C. M. Soukoulis, Determination of Effective Permittivity and Permeability of Metamaterials from Reflection and Transmission Coefficients, *Phys. Rev. B: Condens. Matter Mater. Phys.*, 2002, **65**(19), 195104.

39 J. M. Soler, E. Artacho, J. D. Gale, A. Garcia, J. Junquera, P. Ordejon and D. Sanchez-Portal, The SIESTA Method for Ab Initio Order-N Materials Simulation, *J. Phys.: Condens. Matter*, 2002, **14**(11), 2745–2779.

40 J. P. Perdew, K. Burke and M. Ernzerhof, Generalized Gradient Approximation Made Simple, *Phys. Rev. Lett.*, 1997, **78**(7), 1396.

41 R. G. Quhe, R. X. Fei, Q. H. Liu, J. X. Zheng, H. Li, C. Y. Xu, Z. Y. Ni, Y. Y. Wang, D. P. Yu, Z. X. Gao and J. Lu, Tunable and Sizable Band Gap in Silicene by Surface Adsorption, *Sci. Rep.*, 2012, **2**, 853.

42 Y. Liang and L. Yang, Carrier Plasmon Induced Nonlinear Band Gap Renormalization in Two-Dimensional Semiconductors, *Phys. Rev. Lett.*, 2015, **114**(6), 063001.

43 Y. Zhang, T. R. Chang, B. Zhou, Y. T. Cui, H. Yan, Z. Liu, F. Schmitt, J. Lee, R. Moore, Y. Chen, H. Lin, H. T. Jeng, S. K. Mo, Z. Hussain, A. Bansil and Z. X. Shen, Direct Observation of the Transition from Indirect to Direct Bandgap in Atomically Thin Epitaxial $MoSe_2$, *Nat. Nanotechnol.*, 2014, **9**(2), 111–115.

44 Y. Pan, Y. Dan, Y. Wang, M. Ye, H. Zhang, R. Quhe, X. Zhang, J. Li, W. Guo, L. Yang and J. Lu, Schottky Barriers in Bilayer Phosphorene Transistors, *ACS Appl. Mater. Interfaces*, 2017, **9**(14), 12694–12705.

45 Y. Y. Liu, P. Stradins and S. H. Wei, van der Waals Metal-Semiconductor Junction: Weak Fermi Level Pinning Enables Effective Tuning of Schottky Barrier, *Sci. Adv.*, 2016, **2**(4), e1600069.

46 X. F. Qian, J. W. Liu, L. Fu and J. Li, Quantum Spin Hall Effect in Two-Dimensional Transition Metal Dichalcogenides, *Science*, 2014, **346**(6215), 1344–1347.

47 Y. Y. Wang, R. X. Yang, R. Quhe, H. X. Zhong, L. X. Cong, M. Ye, Z. Y. Ni, Z. G. Song, J. B. Yang, J. J. Shi, J. Li and J. Lu, Does P-Type Ohmic Contact Exist in WSe_2-Metal Interfaces?, *Nanoscale*, 2016, **8**(2), 1179–1191.

48 H. Zhong, R. Quhe, Y. Wang, Z. Ni, M. Ye, Z. Song, Y. Pan, J. Yang, L. Yang, M. Lei, J. Shi and J. Lu, Interfacial Properties of Monolayer and Bilayer MoS_2 Contacts with Metals:

Beyond the Energy Band Calculations, *Sci. Rep.*, 2016, **6**, 21786.

49 Z.-Q. Fan, X.-W. Jiang, J.-W. Luo, L.-Y. Jiao, R. Huang, S.-S. Li and L.-W. Wang, In-Plane Schottky-Barrier Field-Effect Transistors Based on 1T/2H Heterojunctions of Transition-Metal Dichalcogenides, *Phys. Rev. B*, 2017, **96**(16), 165402.

50 Z. Y. Ni, M. Ye, J. H. Ma, Y. Y. Wang, R. G. Quhe, J. X. Zheng, L. Dai, D. P. Yu, J. J. Shi, J. B. Yang, S. Watanabe and J. Lu, Performance Upper Limit of sub-10 nm Monolayer MoS_2 Transistors, *Adv. Electron. Mater.*, 2016, **2**(9), 1600191.

51 R. G. Quhe, Y. Y. Wang, M. Ye, Q. X. Zhang, J. Yang, P. F. Lu, M. Lei and J. Lu, Black Phosphorus Transistors with van der Waals-Type Electrical Contacts, *Nanoscale*, 2017, **9**(37), 14047–14057.

52 H. Li, X. Yan, G. F. Luo, R. Qin, Q. H. Liu, L. L. Yu, C. Y. Xu, J. X. Zheng, J. Zhou, J. Lu, Z. X. Gao, S. Nagase and W. N. Mei, Functionalized Metallic Single-Walled Carbon Nanotubes as a High-Performance Single-Molecule Organic Field Effect Transistor: An ab Initio Study, *J. Phys. Chem. C*, 2010, **114**(37), 15816–15822.

53 P. F. Qi, A. Javey, M. Rolandi, Q. Wang, E. Yenilmez and H. J. Dai, Miniature Organic Transistors with Carbon Nanotubes as Quasi-One-Dimensional Electrodes, *J. Am. Chem. Soc.*, 2004, **126**(38), 11774–11775.